JMEPEG (2022) 31:7018–7030
https://doi.org/10.1007/s11665-022-06679-7

1059-9495/$19.00

TECHNICAL ARTICLE

Characterization of Hydrogen Diffusion in Offshore Steel S420G2+M Multi-layer Submerged Arc Welded Joint

Michael Rhode, Jonathan Nietzke, Tobias Mente, Tim Richter, and Thomas Kannengiesser

Submitted: 29 October 2021 / Revised: 1 December 2021 / Accepted: 4 January 2022 / Published online: 28 February 2022

As onshore installation capacity is limited, the increase in the number of offshore wind turbines (OWT) is a major goal. In that connection, the OWTs continuously increase in size and weight and demand adequate foundations concepts like monopiles or tripods. These components are typically manufactured from welded mild steel plates with thickness up to 200 mm. The predominant welding technique is submerged arc welding (SAW). In accordance with the standards, the occurrence of hydrogen-assisted cracking is anticipated by either a minimum waiting time (MWT, before non-destructive testing of the welded joint is allowed) at ambient or a hydrogen removal heat treatment (HRHT) at elevated temperatures. The effectiveness of both can be estimated by calculation of the diffusion time, i.e., diffusion coefficients. In this study, these coefficients are obtained for the first time for a thick-walled S420G2+M offshore steel grade and its multi-layer SAW joint. The electrochemical permeation technique at ambient temperature is used for the determination of diffusion coefficients for both the base material and the weld metal. The coefficients are within a range of 10^{-5} to 10^{-4} mm^2/s (whereas the weld metal had the lowest) and are used for an analytical and numerical calculation of the hydrogen diffusion and the related MWT. The results showed that long MWT can occur, which would be necessary to significantly decrease the hydrogen concentration. Weld metal diffusion coefficients at elevated temperatures were calculated from hydrogen desorption experiments by carrier gas hot extraction. They are within a range of 10^{-3} mm^2/s and used for the characterization of a HRHT dwell-time. The analytical calculation shows the same tendency of long necessary times also at elevated temperatures. That means the necessary time is strongly influenced by the considered plate thickness and the estimation of any MWT/HRHT via diffusion coefficients should be critically discussed.

Keywords energy, hydrogen diffusion, modeling and simulation, steel, welding

1. Introduction

As part of the energy transition and future hydrogen-based economy, the further expansion of power generation by offshore wind turbines (OWT) must be accelerated by number and size. For example, Germany plans to install an additional power 20 GW by 2030 (Ref 1, 2). Currently, the foundations are mostly monopiles (2018: 76% of installed OWT) (Ref 3).

This article is an invited submission to the *Journal of Materials Engineering and Performance* selected from presentations at the symposium "Joining," belonging to the area "Processing" at the European Congress and Exhibition on Advanced Materials and Processes (EUROMAT 2021), held virtually from September 12–16, 2021, and has been expanded from the original presentation.

Michael Rhode, Jonathan Nietzke, and **Thomas Kannengiesser**, Department 9 - Component Safety, Bundesanstalt für Materialforschung und -prüfung (BAM), Unter den Eichen 87, 12205 Berlin, Germany; and Institute for Materials Science and Joining Technology, Otto-von-Guericke-University, Universitätsplatz 2, 39106 Magdeburg, Germany; **Tobias Mente** and **Tim Richter**, Department 9 - Component Safety, Bundesanstalt für Materialforschung und -prüfung (BAM), Unter den Eichen 87, 12205 Berlin, Germany. Contact e-mail: michael.rhode@bam.de.

Abbreviations

BM	Base material
CGHE	Carrier gas hot extraction
HAC	Hydrogen-assisted cracking
HAZ	Heat-affected zone
HRHT	Hydrogen removal heat treatment
MWT	Minimum waiting time
SAW	Submerged arc welding
WM	Weld metal

Latin character

a_i	Slope at inflection point, [A/(mm^2*s)]
A	Charging surface area of permeation sample, [mm]
C	(Normalized) Hydrogen concentration, [–] or [%]
D	Temperature dependent diffusion coefficient, [mm^2/s]
D_0	Material dependent diffusion constant, [mm^2/s]
D_{CGHE}	Diffusion coefficient at elevated temperatures, determined by CGHE, [mm^2/s]
D_{Lag}	Time-lag diffusion coefficient, [mm^2/s]
D_{IP}	Inflection point diffusion coefficient, [mm^2/s]
$D_{min,\ BM}$	Minimum base material diffusion coefficient, [mm^2/s]
$D_{min,\ WM}$	Minimum weld metal diffusion coefficient, [mm^2/s]
$D_{max,BM}$	Maximum base material diffusion coefficient, [mm^2/s]

$D_{max,\ WM}$	Maximum weld metal diffusion coefficient, [mm^2/s]
E_A	Activation energy, [kJ/mol]
F	Faraday constant (96,485.3 As/mol)
i_{max}	Maximum permeation current density, [A/mm^2]
$i_{(t)}$	Time-dependent permeation current density, [A/mm^2]
I	Permeation current, [A]
$J_{(t)}$	Time-dependent hydrogen flux, [mol/(mm^2*s)]
J_{max}	Maximum hydrogen flux, [mol/(mm^2*s)]
L	Sample thickness/diffusion length, [mm]
L_{C1}	Characteristic diffusion length 1, [mm]
L_{C2}	Characteristic diffusion length 2, [mm]
R	Universal gas constant (8.31 J/(K*mol))]
t	Time
T	Temperature, [K] or [°C]
$t_{0.5}$	Time after 50% of hydrogen desorbed /effused, [s]
t_{lag}	Time-lag time, [s]
z	Number of transferred electrons, [–]

Greek characters

Φ	Permeability (in steady-state condition), [mol/(mm*s)]
τ	Dimensionless time, [–]

These large structures are erected from submerged arc welded (SAW) components that are made from high-strength offshore steels. In this context, modern thermomechanical-rolled steels, such as S420G2+M, offer improved weldability (e.g., through a lowered carbon equivalent) with simultaneously excellent mechanical properties. The improved weldability enables the welding of these steels without preheating. The underlying standards for the construction include so-called minimum waiting time (MWT) before the necessary non-destructive testing can be performed (Ref 4) to safely exclude hydrogen-assisted cracking (HAC) of the welded joints (Ref 5). The MWT results in long time intervals in which the components must "rest" and thus influence the manufacturing costs. A MWT reaches from 24 h (yield strength of less than 460 MPa) (Ref 5) up to 48 h (Ref 6). The time-delayed HAC is the result of a critical combination of: (1) hydrogen concentration, (2) mechanical stresses in (3) a susceptible microstructure (Ref 7). In that connection, thick steel plate welded joints imply some special issues that can increase the susceptibility for HAC and have to be considered: substantially extended diffusion paths for the hydrogen, regions with high weld residual stresses, high local strains, and hardened regions in the HAZ. Possible sources of hydrogen are, for example, moisture welding flux or condensates on the plate surface. However, such known hydrogen sources can be largely eliminated before and during welding, e.g., by "soaking" or "bake-out" of the welding consumables and keeping the material surface clean (removal of grease, scale, avoidance of condensates) (Ref 8, 9). In addition, it is possible to reduce any critical hydrogen concentrations that may be present in the welds, by heat treatment after welding. This process is called hydrogen removal heat treatment—HRHT (also referred as Dehydrogenation Heat Treatment-DHT) (Ref 10-12). As a beneficial effect, this would also eliminate the need for MWT.

However, the procedures must still be economically viable. The necessary HRHT dwell time and temperature depend, among other things, on the sheet thickness and can be estimated using diffusion coefficients by analytical or numerical calculations. However, a problem must be considered, namely that for high-strength steels with similar chemical compositions, deviations in the diffusion coefficients of up to three orders of magnitude are found for ambient temperature (Ref 13). Chemically similar base materials (BM), such as low-alloy pipeline steels, are in the range of 10^{-4} mm^2/s (Ref 14, 15) and thus up to one order of magnitude higher. Thus, mere base material considerations are not suitable for estimating a MWT or even the dwell time for a HRHT. However, the literature contains hardly any statements on pure weld metal (WM) for the relatively new offshore steel grade S420G2+M and suitable SAW consumables. Gas metal arc welding (GMAW) tests resulted in a typical initial hydrogen concentration of maximum 5 ml/100 g Fe, i.e., H5 classification (Ref 16). It is believed that this would be a realistic concentration also for SAW joints. In that connection, available diffusion coefficients of the WM lie within the range of 10^{-5} mm^2/s (Ref 17).

Therefore, the focus of this study is the determination of the hydrogen diffusion in a SAW multi-layer joint of the offshore steel grade S420G2+M. Its good weldability and related welding parameter sets are well known (Ref 16, 18). With the scope on HAC, the microstructure-dependent hydrogen diffusion coefficients (BM and WM) had been determined the first time for this steel grade. For that purpose, two experimental methods were used: (1) permeation experiments at ambient temperature and (2)—for the first time—for the WM in the range of 120 to 400 °C via carrier gas hot extraction (CGHE). Based on the analytical calculations, case studies show the importance of diffusion coefficients for MWT and HRHT. In addition, a numerical calculation was conducted to simulate the combined hydrogen diffusion in the welded joint using the microstructure-dependent diffusion coefficients of WM and BM.

2. Materials and Methods

2.1 Welding Experiments and Sample Extraction

A multi-layer SAW joint has been delivered by a project partner for the machining of samples or the characterization of the diffusion, within the BM and WM. For that purpose, the BM was a 60 mm thick plate of S420G2+M (Ref 19). The joint was welded by means of a multi-wire process. The SAW welding wire and flux combination consisted of the 4-mm-diameter OE-SD3 solid wire (Ref 20) and agglomerated alkaline welding flux OP121TT (Ref 21). The BM and the filler metal/flux combination are optimized for offshore applications. The chemical composition is shown in Table 1 (BM and WM after deposition and analyzed by optical emission spectroscopy, welding flux in accordance with manufacturer's specification).

The joint was welded in PA position, and the welded joint geometry is shown in Fig. 1(a). For a proper weld heat input, a preheating temperature of ≥ 15 °C and an interpass temperature of ≤ 250 °C was maintained. The welding edge preparation consisted of a Y-groove preparation with 60° opening angle (starting at ¼ of the plate thickness, referred to side B). For this purpose, the welding sequence encompassed: first and second step: welding of five filler layers and three cover layers,

then side A was counter-milled starting with a flank angle of 10° and then side A was welded with twelve filler layers as third step and final welding of four cover layers as fourth step. The filler layers were welded with 5-wire technology and the cover layers with 3-wire technology (530 to 640 A, 31 to 34 V, 1500 to 2000 mm/min). This resulted in a weld heat input of about 25 to 30 kJ/cm. Pure BM and WM blocks with 120 mm length and 10 mm width were extracted (see Fig. 1b). Subsequently, the samples were machined from the blocks with the sample geometries shown in Fig. 1(c) (permeation) and Fig. 1(d) (carrier gas hot extraction - GGHE).

2.2 Determination of Diffusion Coefficients Via Electrochemical Permeation and Carrier Gas Hot Extraction

2.2.1 Electrochemical Permeation/Base Material and Weld Metal Diffusion Coefficients at Ambient Temperature. The method is widely used to determine hydrogen diffusion in metals (Ref 22). More detailed information on the experimental method is shown, for example, in (Ref 23). The basic setup consists of an electrochemical double cell with the cathode and anode half-cell separated by the sample under investigation, see Fig. 2(a). Figure b and c shows two evaluation methods for the calculation of the diffusion coefficients. All investigations were performed at ambient temperature (21 °C). Sample thicknesses of 0.50 mm and 1.00 mm were used for the experiments to evaluate a thickness effect.

The cathodic side (−) was filled with an acidic solution of 0.1 M H_2SO_4 and 0.05 M $NaAsO_2$ (as recombination inhibitor) and a galvanic current density of 1.25 mA/cm^2 was applied. The anodic (+) side for hydrogen detection was filled with a 0.1 M NaOH solution and potentiostatically polarized at +200 mV against Ag/AgCl reference electrode (Xylem SI Analytics). The desorbing H^+ protons reduce the OH^- hydroxide ions to H_2O. This oxidation current "I" (in A) resulting from the electron transfer is recorded with a digital multimeter with a step size of 1 s. It is additionally converted into the permeation current density "i" (in A/mm^2, Eq 1) by division of the current trough the permeation area (circle, "A" = 200 mm^2). By Faraday's law (with F = 96,485.3 As/mol (Ref 24)), this can be converted into a hydrogen flux "J" (in mol/(mm^2*s), Eq 2). The constant "z" in Eq 2 corresponds to the number of transferred electrons (=1). The permeability "ϕ" (in mol/(mm*s), Eq 3) is the maximum achieved current density along the sample thickness "L" and is a measure for the hydrogen permeability. The diffusion coefficient was calculated using two different methods: (1) The time-lag method (Ref 22) (Fig. 2b) determines the time "t_{Lag}" (in s) after which 63% of the maximum permeation current density has been reached to calculate the "D_{Lag}" (in mm^2/s, Eq 4) and (2) the inflection point method according to (Ref 23) (Fig. 2c) interprets the slope of the rising permeation transient. For this purpose, the inflection point "a_i" (Eq 5) and the "D_{IP}" (in mm^2/s, see Eq 6) are calculated.

$$i_{(t)} = I/A \quad \text{(Eq 1)}$$

Time-dependent permeation current density

$$J_{(t)} = i_{(t)}/(z * F) \quad \text{(Eq 2)}$$

Time-dependent hydrogen flux

$$\Phi = J_{\max} * L \quad \text{(Eq 3)}$$

Permeability (in steady-state condition)

$$D_{\text{Lag}} = L^2/(6 * t_{\text{Lag}}) \quad \text{(Eq 4)}$$

Timelag diffusion coefficient

$$a_i = \mathrm{d}i/\mathrm{d}t \quad \text{(Eq 5)}$$

Slope at inflection point

$$D_{\text{IP}} = (0.04124 * L^2 * a_i)/(0.2442 * i_{\max}) \quad \text{(Eq 6)}$$

Inflection point diffusion coefficient

2.2.2 Carrier Gas Hot Extraction/Weld Metal Diffusion Coefficients in the Range From 120 to 400 °C. The determination of the diffusion coefficients at higher temperatures was carried out by using the carrier gas hot extraction (CGHE). For this purpose, an infrared oven IR07 and connected analyzer G8 Galileo (both Bruker AXS) with an additional mass spectrometer ESD100 (InProcess Instruments) were used. The samples (2.7 mm edge length, square base, 20 mm length, see Fig. 2d) were electrochemical hydrogen-charged analogous to the permeation. However, the charging time of 48 h was significantly longer here, since the effective length of the diffusion path corresponds to one half the sample thickness $b = L/2$ (of 1.35 mm). This ensures that the hydrogen distribution in the sample is as homogeneous as possible, which is important for the evaluation of the bulk diffusion. For the determination of the diffusion coefficients, the samples were heated to the desired temperature by specially developed rapid heating procedures and kept isothermal. Further information can be found in (Ref 23). The recorded desorption curve was then used to determine the time "$t_{0.5}$" after which 50% of the initial hydrogen has effused from the sample, see Fig. 3. The D_{CGHE} was calculated using Eq 7 according to (Ref 26) or the simplified Eq 8 for a constant b = 1.35 mm (maximum length of diffusion path). For the temperature levels 120, 200, 315 and 400 °C, the mean value was calculated from three measurements. Hydrogen sources during SAW is typically a humid welding flux, for example by insufficient storage conditions and missing redrying before welding. That means the weld seam would be the hydrogen source for HAC. The determination of

Table 1 Chemical composition of base material, welding consumable and flux in wt.%

Material	C	Mn	Si	Cr	Ni	Mo	P+S
Base material (BM)	0.10	1.53	0.51	0.04	0.03	0.01	0.01
Deposited Weld metal (WM)	0.09	1.58	0.31	0.04	0.02	0.01	0.01

Material	SiO_2+TiO_2	CaO + MgO	Al_2O_3	CaF_2	.	.	.
Welding flux	15	40	20	25	.	.	.

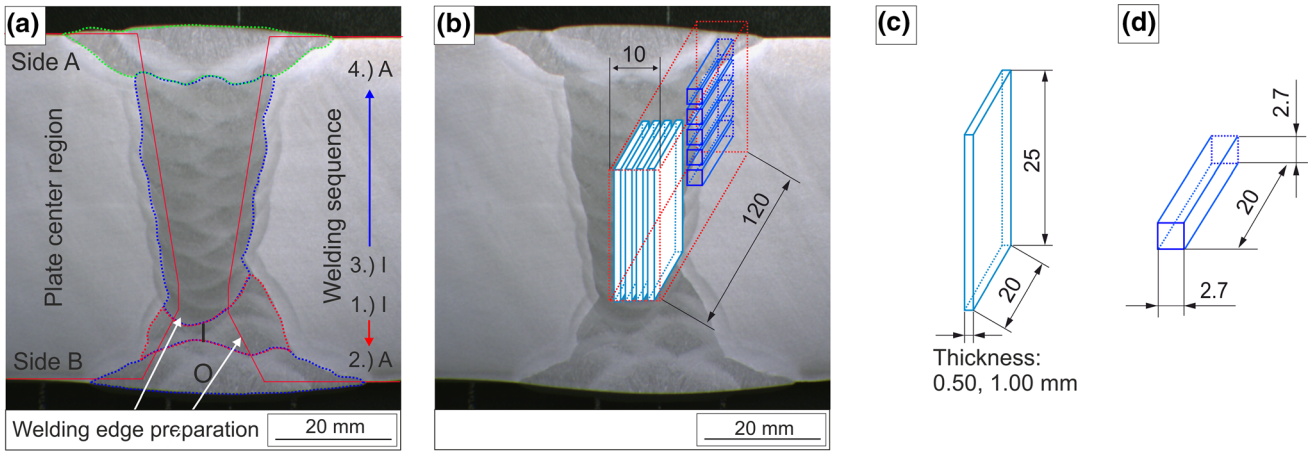

Fig. 1 Specimen geometry: (a) cross section of weld joint, (b) specimen locations of extraction of (c) permeation and (d) carrier gas hot extraction specimens (Color figure online)

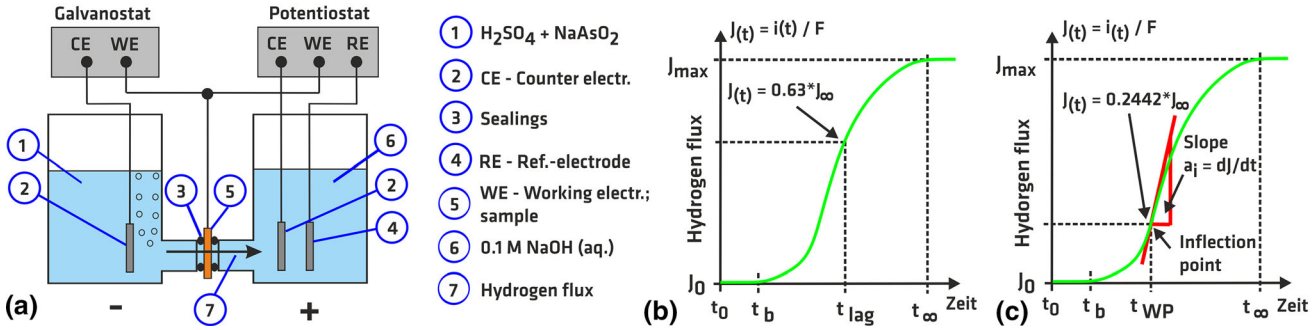

Fig. 2 Electrochemical permeation: (a) experimental setup, (b) time-lag and (c) inflection point method (Color figure online)

high-temperature diffusion coefficients for HRHT is more important for the WM. For that reason, only the WM was regarded.

$$D_{\mathrm{CGHE}} = 0.0492 * L^2/t_{0.5} \qquad \text{(Eq 7)}$$

Temperature dependent diffusion coefficient via CGHE

$$D_{\mathrm{CGHE}} = 0.090\ \mathrm{mm}^2/t_{0.5} \qquad \text{(Eq 8)}$$

Simplified diffusion coefficient for L = 1.35 mm

2.3 Numerical Simulation of MWT/Hydrogen Diffusion at Ambient Temperature

Permeation experiments were used to determine hydrogen diffusion characteristics and to calculate the corresponding coefficients. The finite element software ANSYS was used to simulate the microstructure-dependent diffusion in the SAW joint by using the previously determined coefficients. The aim was to identify the need for the MWT after welding by analyzing the local AND time-dependent decrease in the hydrogen concentration in the cross-section of the welded joint. The reason is that these specific values determine a certain HAC susceptibility (Ref 7, 8). For that purpose, a two-dimensional model of the weld geometry in Fig. 1(a) was created. The model was generated and meshed using APDL (ANSYS Parametric Design Language) as shown in Fig. 4. In this process, a two-dimensional model is generated via so-

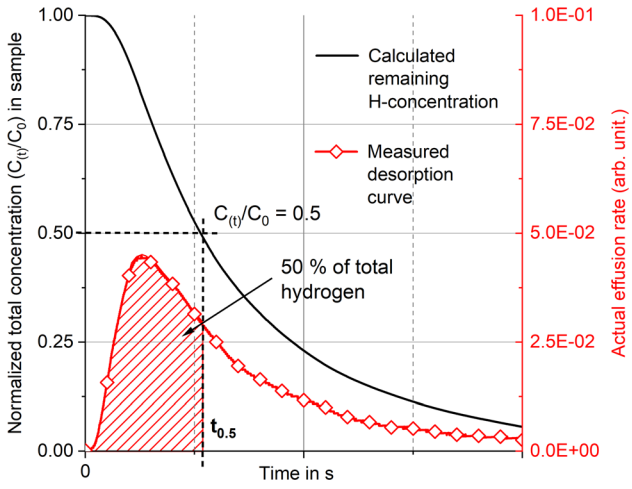

Fig. 3 Determination of DC at elevated temperatures via CGHE (Color figure online)

called key points and then meshed. For that purpose, the Plane55 element was used (two-dimensional thermal solid element with four knots and one degree of freedom per knot). For the simulation of the hydrogen diffusion and distribution, the analogy of Fourier's heat conduction differential equation and Fick's second law (Ref 27), the temperature field simulation module in ANSYS was used. This can be performed as neither further hydrogen sources nor sinks are anticipated. That

means the heat flux ($\dot{q}$) can be neglected in the heat conduction differential equation. For that reason, the temperature (T) equals the hydrogen concentration (C) and the thermal conductivity (λ) equals the diffusion coefficient (D). In addition, the material density (ρ) and specific heat capacity (c_p) are set to 1. Further details on this modeling procedure and the implementation of the simulation can be found in (Ref 11, 28). The welding process or HRHT was not simulated, as the focus was here to identify possible MWTs as the critical time-limitation of the component production.

For the simulation of the hydrogen diffusion at ambient temperature after welding was finished it was assumed that hydrogen is homogeneously distributed in the WM. Thus, a normalized initial hydrogen concentration of $C = 1$ (corresponds to 100 %) was set to all the nodes in the WM. Furthermore, free hydrogen effusion was assumed, setting a hydrogen concentration of zero to the corresponding nodes on all free surfaces in the model. For realistic diffusion simulation, the microstructure-dependent diffusion coefficients of both BM and WM had been combined in the model (see Fig. 4). To assess the minimum and maximum calculated MWT, the corresponding D_{min} and D_{max} of the BM and WM (section 3.1) had been applied. Due to the estimated time of several hours to days, the time-step resolution was set to 600 s.

3. Results and Discussion

3.1 Diffusion Coefficients

3.1.1 Electrochemical Permeation, Diffusion at Ambient Temperature. The results of the electrochemical permeation experiments are shown in Fig. 5 for both BM and WM. Parts a and b show the absolute data, and parts c and d show the corresponding normalized experimental data. The characteristic permeation values and calculated diffusion coefficients are shown in Table 2.

Figure 5 shows that all permeation experiments follow a similar time course. The so-called permeation transients show a certain time until the first hydrogen is detected, then increase exponentially and reach a plateau value (steady-state condition). Here, the effect of the sample thickness can be seen from the maximum permeation current density or from the time course of reaching the plateau value. With increasing specimen thickness, the maximum permeation current density or permeability generally decreases. The calculated diffusion coefficients (D_{Lag} and D_{IP}, see Table 2) show a small deviation for the respective examined thickness-microstructure combination. Some points had been observed for the calculated diffusion coefficients:

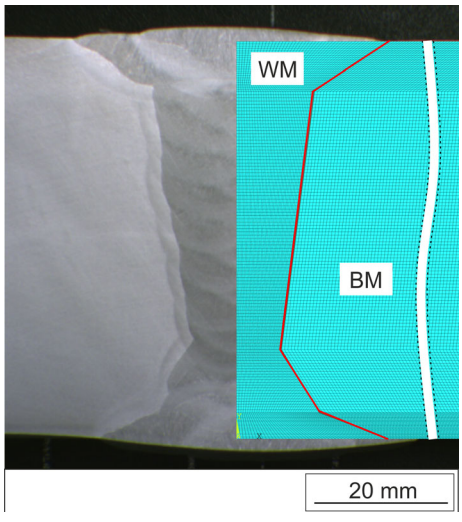

Fig. 4 Real weld seam (left) and numerical two-dimensional model with areas for application of different DCs for WM and BM, red line represents assumed (simplified) solidification line (Color figure online)

Generally, the 0.50 mm thickness resulted in decreased diffusion coefficients compared to 1.00 mm. The change of diffusion coefficients with the sample thickness was previously reported in (Ref 23, 29) but should be actually independent of it according to Fick's diffusion laws. However, this is only an apparent contradiction since experimental boundary conditions (adsorption reactions) have to be considered. If the sample is relatively thin, the adsorption kinetics for the hydrogen from any electrochemical charging media may outweigh the actual permeation/diffusion measurement and result in unrealistic small values for the diffusion coefficients. This means that relatively thick samples (1.00 mm) should be used for the permeation experiments. Accordingly, the higher diffusion coefficients of the 1.00 mm thickness are better suited to describe the hydrogen diffusion and should indicate a relatively rapid hydrogen concentration decay in a S420 SAW joint.

If the different microstructure is considered, the BM showed the higher calculated diffusion coefficients compared the WM (approximately by factor 2). The explanation is the different annealing condition and texture of the microstructure. The BM represents a very homogenous annealed microstructure due to the hot-rolling, in contrast to the multi-layer welding process of the WM. The repeated thermal cycling causes complex recrystallization, grain growth, dissolution, and re-precipitation of carbides and in the WM, which increases the number of hydrogen traps significantly, i.e., decreases the diffusivity by binding hydrogen. Compared to pure iron, any low-alloyed steel is already a complex microstructure in terms of hydrogen traps. Possible trapping effects are already covered by the calculated diffusion coefficients. These are commonly referred as "effective" diffusion coefficients (Ref 15, 22, 23), although this term is not used in the present study. It is very complex to distinguish already between lattice diffusion and the specific share of the traps, which delay the hydrogen concentration.

In addition, the so-called apparent diffusion coefficient must be distinguished in case of permeation experiments. The reason is that the adsorption is necessary boundary condition for the permeation. That means the time-lag and inflection point method should result insignificantly different diffusion coefficients, despite the same sample geometry (Ref 23, 29). But the typical advantage of the inflection point method to neglect hydrogen adsorption reactions does not account in our case and both methods resulted in similar coefficients for a respective thickness-microstructure-combination. From our point of view, this is due to the relatively fast hydrogen diffusion in both the BM and WM, i.e., the short time to the first hydrogen detection of maximum 200 s (BM) or 400 s (WM), i.e., negligible in contrast to the total permeation experiment time. In the overall consideration, the diffusion coefficients are up to one order of magnitude apart: minimum with $4.31*10^{-5}$ mm^2/s (D_{min}; 0.50 mm) and maximum $17.4*10^{-5}$ mm^2/s (D_{max}; 1.00 mm). For 0.50 mm, they are thus comparable to literature values

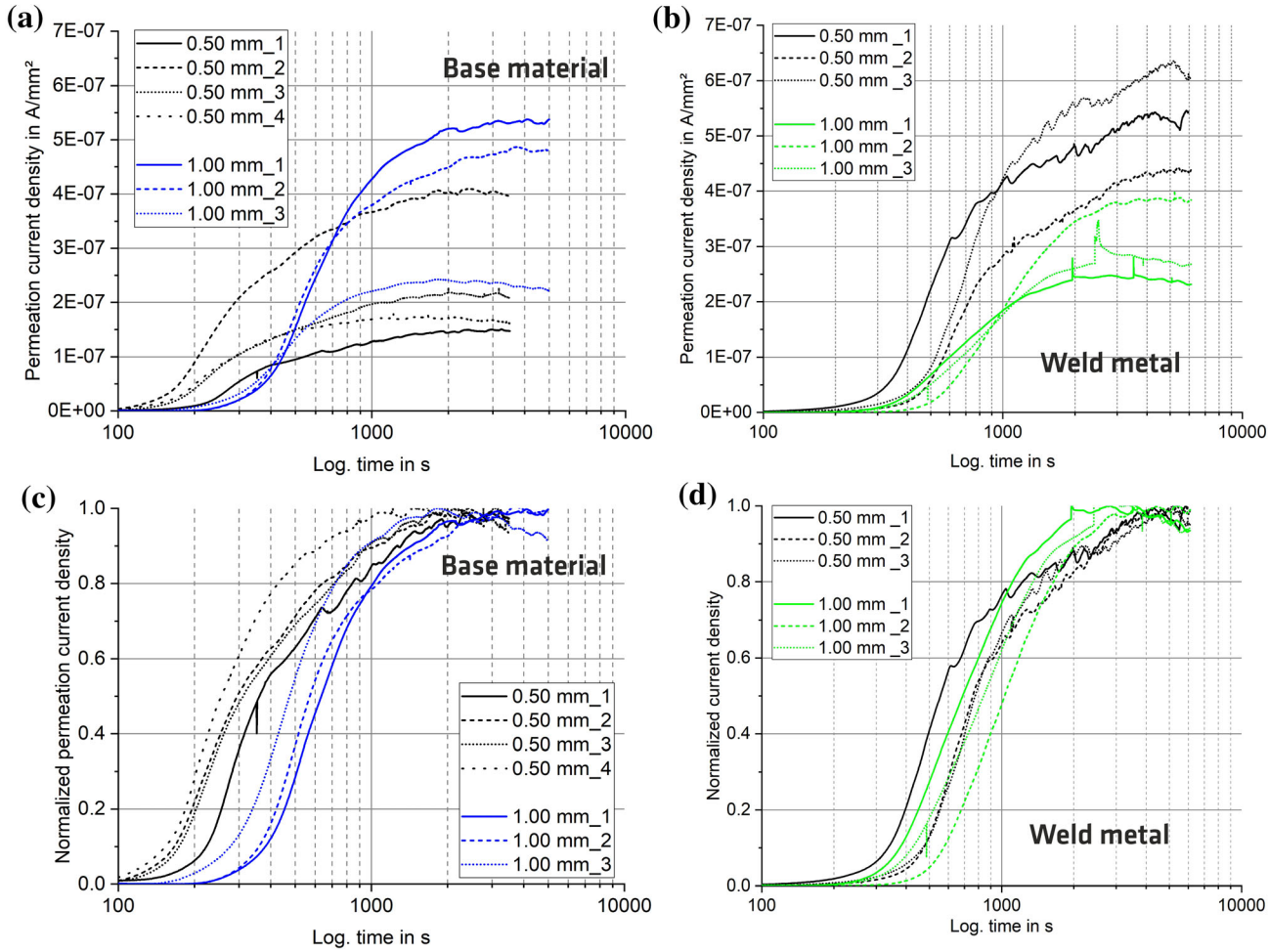

Fig. 5 Diffusion at room temperature: (a) BM and (b) WM, corresponding normalized data is shown in (c) BM and (d) WM (Color figure online)

Table 2 Measured permeation values and calculated diffusion coefficients at ambient temperature for BM and WM

Material	L in mm	i_{max} in 10^{-7} A/mm^2	ϕ in 10^{-12} mol/mm*s	t_{lag} in s	a_i in 10^{-10} A/(mm^2*s)	D_{lag} in 10^{-5} mm^2/s	D_{IP} in 10^{-5} mm^2/s
BM	0.50	2.37 ± 1.18	1.23 ± 0.61	410 ± 79	9.70 ± 4.39	9.47 ± 2.15	17.60 ± 2.82
	1.00	4.22 ± 1.57	4.37 ± 1.63	657± 98	8.51 ± 0.75	25.80 ± 4.05	34.60 ± 2.67
WM	0.50	5.41 ± 0.96	5.61 ± 0.97	882 ± 154	5.56 ± 1.52	4.83 ± 0.94	4.31 ± 0.77
	1.00	3.05 ± 0.74	3.16 ± 0.78	1.030 ± 192	3.04 ± 1.95	16.60 ± 3.11	17.40 ± 3.34

(10^{-5} mm^2/s, according to (Ref 17)) of SAW submerged arc multi-layer WM but are also above them for the 1.00 mm thick specimens. The experimental permeation measurements provide, for the first time, microstructure-dependent diffusion coefficients for hydrogen diffusion in a submerged arc multi-layer WM and BM of an S420G2+M grade and allow analytical calculation of diffusion times at ambient temperature. The correlating practical application is the estimation of necessary MWT for the time-delayed HAC, as shown in section 3.2.

3.1.2 Carrier Gas Hot Extraction: Weld Metal Diffusion Coefficients from 120 °C to 400 °C. In case of the CGHE measurement, an "apparent" diffusion coefficient is derived as no adsorption reactions (from the electrochemical hydrogen charging) have to be considered. Nonetheless, it is also labeled as "effective" diffusion coefficient (due to the combined regarding of lattice diffusion and delay by traps). In addition, a possible concentration dependence of the diffusion coefficient is not anticipated in the case of CGHE as the electrochemical charging conditions ensured a mostly uniform hydrogen distribution in the sample. The results for the WM are shown in Fig. 6 for 120 and 315 °C (for clarity) and are evaluated according to Fig. 3 and Eq 8, respectively. The $t_{0.5}$-times and D_{CGHE} for the WM are shown in Table 3.

From Fig. 6, it can be seen that the effusion curves are subjected to a temperature dependence. The calculated coefficients (Table 3) increase by a factor of 1.2 to 1.3 per 100 °C temperature increment. The coefficient at 400 °C is similar to

the temperature step of 315 °C. The reason is based on the very fast diffusion and the thus limited application of the fast-heating procedure according to (Ref 23). Compared to the permeation experiments at ambient temperature, the diffusion coefficient at 120 °C (depending on the comparative permeation value) are already one to two orders of magnitude higher, i.e., the hydrogen diffuses much faster than at ambient temperature. However, it must be mentioned here as a restriction that desorption (i.e., already occupied traps) is considered for CGHE and adsorption (i.e., the traps are occupied) is primarily considered for permeation. Due to the different experimental methodology, the coefficients are therefore only comparable to a limited extent. When classified in the known scatterband for diffusion coefficients (Ref 13), they are situated in the upper region of the scatterband. This also indicates that the hydrogen in the multi-layer WM diffuses faster than expected. This can also be seen from the activation energy "E_A" in kJ/mol of the diffusion, which can be used, for example, to characterize the prevailing hydrogen traps (Ref 30, 31). For this purpose, the mean values of the diffusion coefficients are plotted above the inverse absolute temperature in a semilogarithmic Arrhenius-plot, see Fig. 7 and in accordance with Eq 9, and E_A can be determined from the slope of the regression function. Here, "D_0" is a specific constant (in mm^2/s) and "R" is the universal gas constant (8.31 J/K * mol) and "T" is the absolute temperature (in K).

$$D = D_0 * e_A^{-(E/(R*T))} \quad \text{(Eq 9)}$$

Temperature dependent D within 120 to 315 °C

Figure 7 shows the regression line between the diffusion coefficients of the temperature from 120 to 315 °C. The temperature of 400 °C was not included in the Arrhenius-plot, since this diffusion coefficients is almost identical to the temperature step of 315 °C. The calculated activation energy E_A of about 4.6 kJ/mol in the temperature range from 120 to 315 °C supports the hypothesis of very rapid diffusion and corresponds to very weakly trapped hydrogen (Ref 10, 30, 31). Strong hydrogen traps (such as grain boundaries, carbides, etc.) in the WM thus play only a minor role in this temperature range. Analogous to the permeation experiments, the diffusion coefficients at higher temperatures allow the calculation of corresponding time for hydrogen diffusion. The practical application here is the subsequent HRHT of the welded joint by the estimation of dwell times and the possible MWT avoidance (Ref 5).

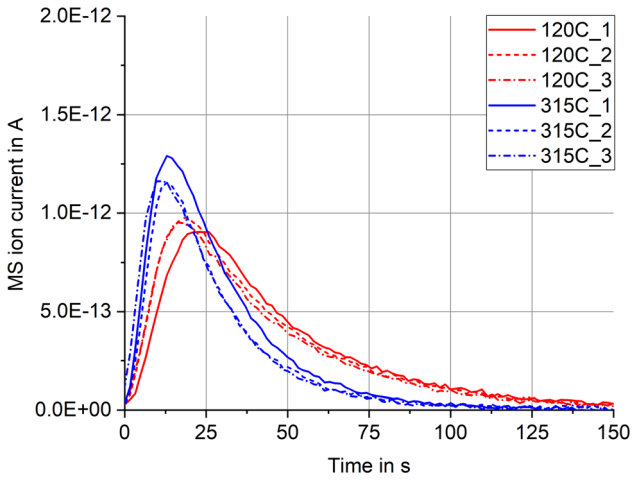

Fig. 6. Examples for effusion curves at 120 °C and 315 °C (Color figure online)

3.2 Analytical Description of Diffusion at Ambient Temperature and from 120 to 400 °C

The temperature dependence of the diffusion can be used to model the decrease in a virtual hydrogen concentration in a welded joint. For this purpose, the weld seam is assumed to be an infinite plate and one-dimensional diffusion through this plate is considered. The analytical approach according to (Ref 8) is used to model the concentration curves. Figure 8(a) shows the underlying assumption that the remaining concentration follows an exponential course, which can be described by the relationship between the diffusion coefficient, hereafter referred as "D," the characteristic length "L_C" (half weld width or thickness) and diffusion time "t," via the so-called dimensionless time "τ" (see Eq 10). This is then used to calculate the decrease in initial concentration after this finite time.

$$\tau = (D * t)/L_C^2 \quad \text{(Eq 10)}$$

Dimensionless time "τ"

From the representation in Fig. 8(a), the values for "τ" are determined for a respective remaining hydrogen concentration. From the "τ" value, the corresponding diffusion time "t" is determined by converting Eq 10. This time can then be

Table 3 Measured $t_{0.5}$-time and calculated diffusion coefficients (D_{CGHE}) for the WM

Temperature in °C	$t_{0.5}$-time in s	D_{CGHE} in 10^{-3} mm^2/s
120	33.4 ± 1.8	2.69 ± 0.14
200	25.4 ± 2.0	3.55 ± 0.28
315	20.9 ± 1.4	4.31 ± 0.30
400	21.1 ± 1.7	4.27 ± 0.34

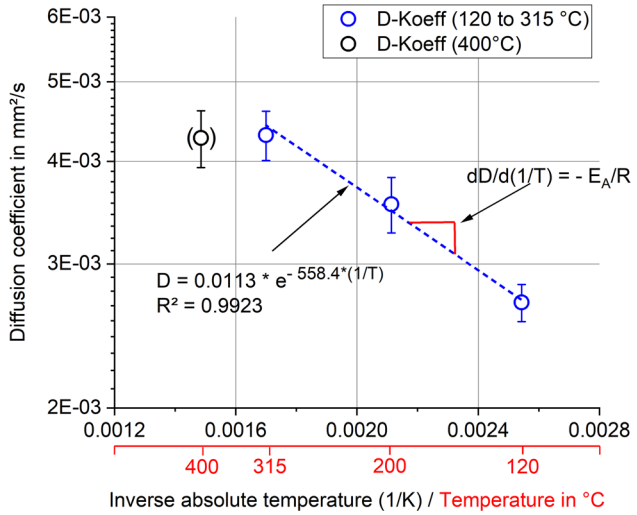

Fig. 7 Arrhenius-Plot for calculation of the activation energy *EA* (Color figure online)

assigned to the originally specified hydrogen concentration. The course of the concentration over the diffusion time can be represented by an exponential regression function between the data points, see Fig. 8(b). Normally, assuming a uniform hydrogen introduction per bead, the concentration is highest in the last layer of a multi-layer weld. Due to the short diffusion paths to the free surface, the concentration in these areas initially reduces rapidly and the range of maximum H concentration shifts to the center of the weld with increasing time. For this purpose, two characteristic lengths L_C for a plate are considered. In each case, L_C is half the plate thickness. L_{C1} is 10 mm, based on the average weld width of approx. 20 mm, and L_{C2} is 30 mm, based on the plate or weld thickness of 60 mm. The values represent maximum possible diffusion paths, i.e., maximum values in terms of time for the required diffusion time. As described in section 1, there is hardly any literature available on the hydrogen diffusion behavior of the WM of offshore steel grades. The values for the BM can only be transferred to a limited extent due to the differences in the microstructure (Ref 13). As a result of our experiments, validated diffusion coefficients for BM and WM of a S420G2+M are now available. The significance of these data and the analytical approach presented is illustrated by two application cases in the following: (1) MWT and (2) HRHT. For this purpose, the diffusion for L_{C1} and L_{C2} is considered.

3.2.1 Case 1: Estimation of MWT Based on Diffusion at Ambient Temperature. Figure 9(a) and 10(a) shows the normalized curves of hydrogen concentration (100% initial concentration = 1, at time $t = 0$, and 0% after finite time) for L_{C1} = 10 mm and L_{C2} = 30 mm for the respective D_{min} and D_{max} at ambient temperature. Assuming that the initial concentration is maximum at the center of the WM, L_{C1} and L_{C2} can then be applied, respectively. As a further assumption, it is assumed here that due to the shorter path length L_{C1}, diffusion would preferentially occur into the HAZ, see Fig. 9(b) and 10(b). Table 4 shows the derived time "$t_{50\%}$," after which the initial concentration in the center of the seam has dropped to 50% due to diffusion.

As shown in Fig. 9(a) and 10(a), the concentration curves follow a time dependence expressed via the combined effect of the diffusion coefficient and the characteristic length (see Eq 10). For a length/thickness of L_{C1} = 10 mm, theoretically after a time of 23 h (BM) and 47 h (WM) using the highest diffusion coefficients, the virtual concentration has dropped to 50 % or at about 85 h (BM) and 188 h (WM) in the case of the lowest diffusion coefficient. These values increase up to times in the months range at L_{C2} = 30 mm independently of the considered microstructure. Nonetheless, the BM was obvious faster than the WM. For the HAC avoidance, the lower diffusion coefficients should be considered in terms of conservative assessing of HAC susceptibility.

The diffusion times may appear to be very high. The reason is simply the length of the diffusion path. According to the current state of SAW processes as well as appropriate welding consumable and flux combination, a maximum hydrogen amount of 5 ml/100 g Fe hydrogen concentration can be expected in the weld (in accordance with the mostly used H5 classification) (Ref 16, 20). This means that in the ideal case, this concentration would have decreased to 2.5 ml/100 g Fe after 48 h (as recommended MWT). In addition, a noticeable degradation of the mechanical weld properties of a higher-strength S690QL starts from a hydrogen concentration of ≥ 2.6 ml/100g and a S355 steel needs already 8 ml/100 g Fe in the welded joint for significant reduction (Ref 32). For steels of lower strength, the necessary hydrogen concentration for a SAW increases. Assuming the same initial concentration in the welded joint of S420G2+M, there is a lower risk for the SAW compared to S690QL. This means that the MWT could possibly be omitted. However, this statement only refers to the purely qualitative consideration of hydrogen diffusion. Additional effects such as the level of residual stresses in the welds must also be considered. However, even under tightened clamping conditions, i.e., high stiffness, there was no detectable formation of HAC, apart from end crater cracks, which were due to the specimen geometry (Ref 33). The application of the permeation methodology is thus helpful for estimating the necessary diffusion time. But it can lead to significantly prolonged time intervals if very high thicknesses are assumed. HAC can be more or less be excluded if the maximum introduced hydrogen concentration is below the critical hydrogen concentration for the material and the associated weld microstructure. Apparently, this is the case under the industrial conditions of SAW production of components. This means that MWT should at least be critically discussed. Based on the proposed methodology, a relatively simple estimation of a diffusion time is

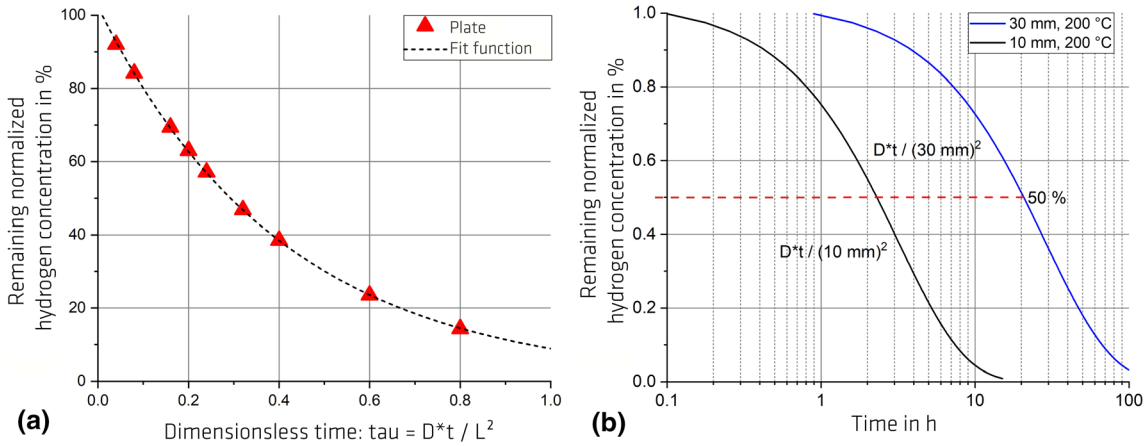

Fig. 8 Decrease in hydrogen concentration: (a) dependency on dimensionless time (Ref 8), (b) examples of derived functions for a plate-like geometry with L_{C1}= 10 mm and L_{C2} = 30 mm under consideration of $D = 3.55*10^{-3}$ mm²/s at 200 °C, see Table 3 (Color figure online)

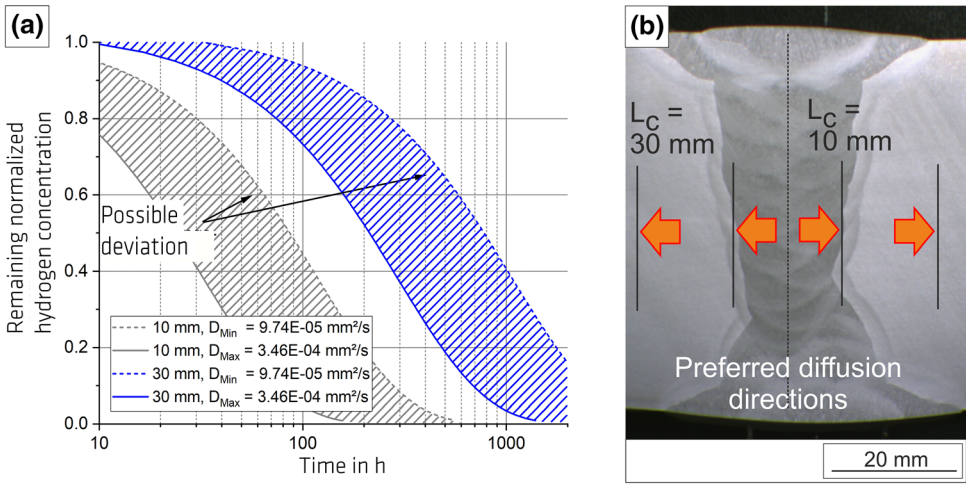

Fig. 9 Estimation of MWT in BM based on DCs at RT: (a) normalized concentration curves for L_{C1} = 10 mm and L_{C2} = 30 mm by consideration of D_{min} or D_{max}, and (b) graphical representation of assumed diffusion direction (Color figure online)

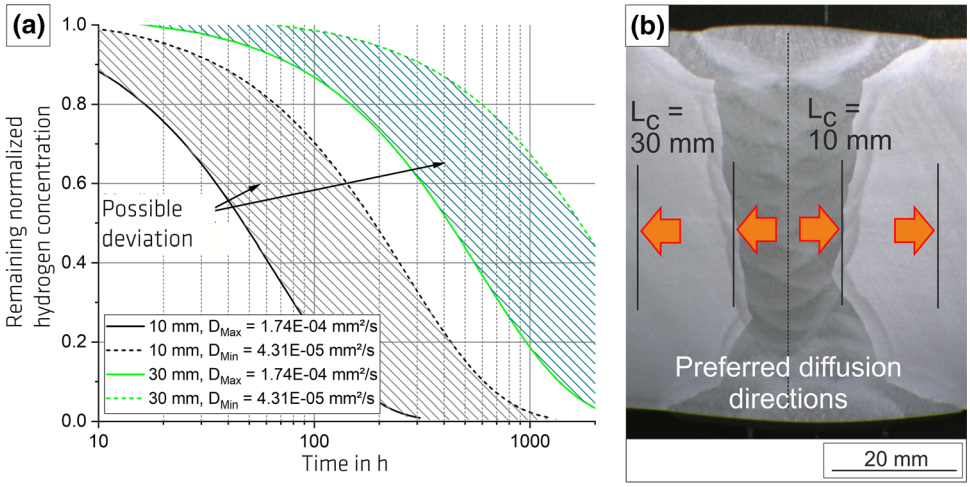

Fig. 10 Estimation of MWT in WM based on DCs at RT: (a) normalized concentration curves for L_{C1} = 10 mm and L_{C2} = 30 mm by consideration of D_{min} or D_{max}, and (b) graphical representation of assumed diffusion direction (Color figure online)

Table 4 Comparison of $t_{50\%}$ times as measure for MWT based on diffusion coefficients for BM and WM

	$t_{50\%}$ [h]	
Specific DC and L_C combination	**BM**	**WM**
D_{max}, L_{C1} = 10 mm	23	47
D_{min}, L_{C1} = 10 mm	85	188
D_{max}, L_{C2} = 30 mm	211	419
D_{max}, L_{C2} = 30 mm	769	1.691

possible (if the diffusion coefficient is known, and the length of the diffusion path).

3.2.2 Case 2: Estimation of Dwell Time for HRHT at Elevated Temperatures. Figure 11(a) shows, analogous to Fig. 9(a) and 10(a), normalized progressions of hydrogen concentration curves determined from the CGHE experiments, for L_{C1} = 10 mm and L_{C2} = 30 mm and diffusion coefficient in the range from 120 to 400 °C. As shown, the diffusion coefficient of 400 °C is very similar to 315 °C. This is likely due to the experimental methodology (limited effectiveness of the rapid heating procedure of the CGHE to allow the hydrogen to desorb from the sample in a defined manner, see (Ref 23)). In addition, this HRHT temperature of 400 °C is not of practical importance for high-strength structural steels since tempering effects (and influences on the mechanical properties) may already be expected. In contrast to the MWT at ambient temperature, higher temperatures are present for/HRHT. Industrial standards for HRHT are, for example, resistance heating mats or burners applied in the weld area. It can be assumed here that hydrogen diffusion occurs preferentially in the direction of the larger temperature gradient, i.e., in the direction of the weld seam/sheet surface. Therefore, in this case, the (half) weld thickness, i.e., L_{C2} = 30 mm is the decisive length for the diffusion path, as indicated in Fig. 9(b) and 10(b). The decrease to 75% of the initial concentration occurs quite rapidly with the calculated diffusion coefficients but increases continuously for a further decrease to 50 % and 25 %, respectively. Table 5 shows the HRHT times for L_{C1} = 10 mm and L_{C2} = 30 mm

after the hydrogen concentration decreased to 50%.

As shown in Fig. 11, at higher temperatures, the calculated diffusion time is much shorter than at ambient temperature. The reason lies in the temperature dependence of hydrogen diffusion, but changes with the length of the diffusion path that is anticipated. A higher temperature is therefore generally helpful for faster, i.e., more effective, reduction of the initial hydrogen concentration. However, a corresponding plate or weld thickness leads to sometimes unrealistically high dwell times. This can be seen, e.g., for L_{C2} = 30 mm as diffusion path length (i.e., 60 mm plate thickness) would require 27.1 h (approximately one day) at 120 °C. The diffusion length L_{C1} = 10 mm (20 mm plate thickness) would require approximately 3.0 h as necessary dwell time. For thin welded joints or seam thickness, the differences in dwell time in the range of 200 to 315 °C (i.e., the typical HRHT recommendation for steels with comparable strength (Ref 11, 12)) are negligible. The temperature of 400 °C cannot be conclusively evaluated based on the presented data but would be more effective (expressed by the shortest dwell time required).

However, it is not recommended from a metallurgical point of view, as local material properties changes (softening due to tempering effects) may already occur in the weld. This is particularly significant for high-strength steels such as S690QL. It remains an open question whether a HRHT is necessary when using adequate filler metals (e.g., H5 classification), even though the use of HRHT is in any case useful for reducing the HAC risk of welded thick plates. Nonetheless, microstructure-dependent diffusion coefficients can be used for simulation of hydrogen diffusion in multi-layer SAW welds and allow a more detailed local modeling in accordance with (Ref 10–12) and is shown in the following section.

3.3 Numerical Analysis of Hydrogen Diffusion in the Welded Joint at Ambient Temperature

The simulation can be used to model the decrease in the hydrogen concentration depending on the diffusion coefficients. In contrast to the analytical calculation in section 3.2., it can show the local hydrogen distribution in the welded joint after certain time using microstructure-dependent diffusion coefficients for BM and WM. For that purpose, the described model (in section 2.3 and Fig. 4) was applied and the hydrogen diffusion with an incremental time of 600 s simulated. Fig. 12 shows selected results for the hydrogen distribution for the fastest diffusion using D_{max} in parts (b–d) and for the slowest diffusion using D_{min} (e–g). In that connection, the part (a) shows the initial concentration in both WM (100%, C = 1) and BM (0%, C = 0). Parts (b) and (e) show the hydrogen distribution after 50% of the initial concentration is reached in the WM, parts (c) and (f) for 25 % and finally (d) and (g) illustrate the situation after 10% is reached. In addition, Table 6 shows the corresponding and necessary diffusion time to reach these values in seconds (s) and days (d).

From Fig. 12, it can be derived that different hydrogen diffusion coefficients mean different diffusion time. Due to the large plate thickness, long diffusion times have to be anticipated independently of the used diffusion coefficients. Nonetheless, the obtained differences in the diffusion coefficients (see Table 2) lead to significant differences in the simulated diffusion time. If the lowest diffusion coefficients are applied ($D_{min,\ BM}$ = 9.47*10^{-5} mm^2/s, $D_{min,\ WM}$ = 4.83*10^{-5} mm^2/s) the necessary decay time to reach 50% of the initial hydrogen concentration is already approximately 16 days or in case of the highest applied diffusion coefficients ($D_{max,\ BM}$ = 34.60*10^{-5} mm^2/s, $D_{max,}$

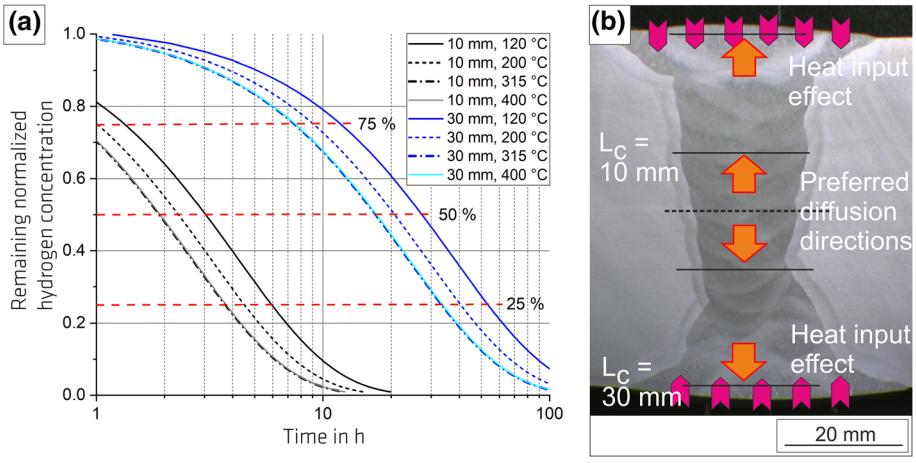

Fig. 11 Estimation of DHT/HRHT dwell time based on elevated temperature DCs for the WM: (a) normalized concentration curves for L_{C1} = 10 and L_{C2} = 30 mm from 120 to 400 °C, (b) of assumed diffusion direction (Color figure online)

Table 5 Estimation of $t_{50\%}$ as measure for dwell time for HRHT

Temperature [°C]	$t_{50\%}$ [h] (L_{C1}=10 mm)	$t_{50\%}$ [h] (L_{C2}=30 mm)
120	3.0	27.1
200	2.3	20.5
315	1.9	16.9
400	1.9	17.1

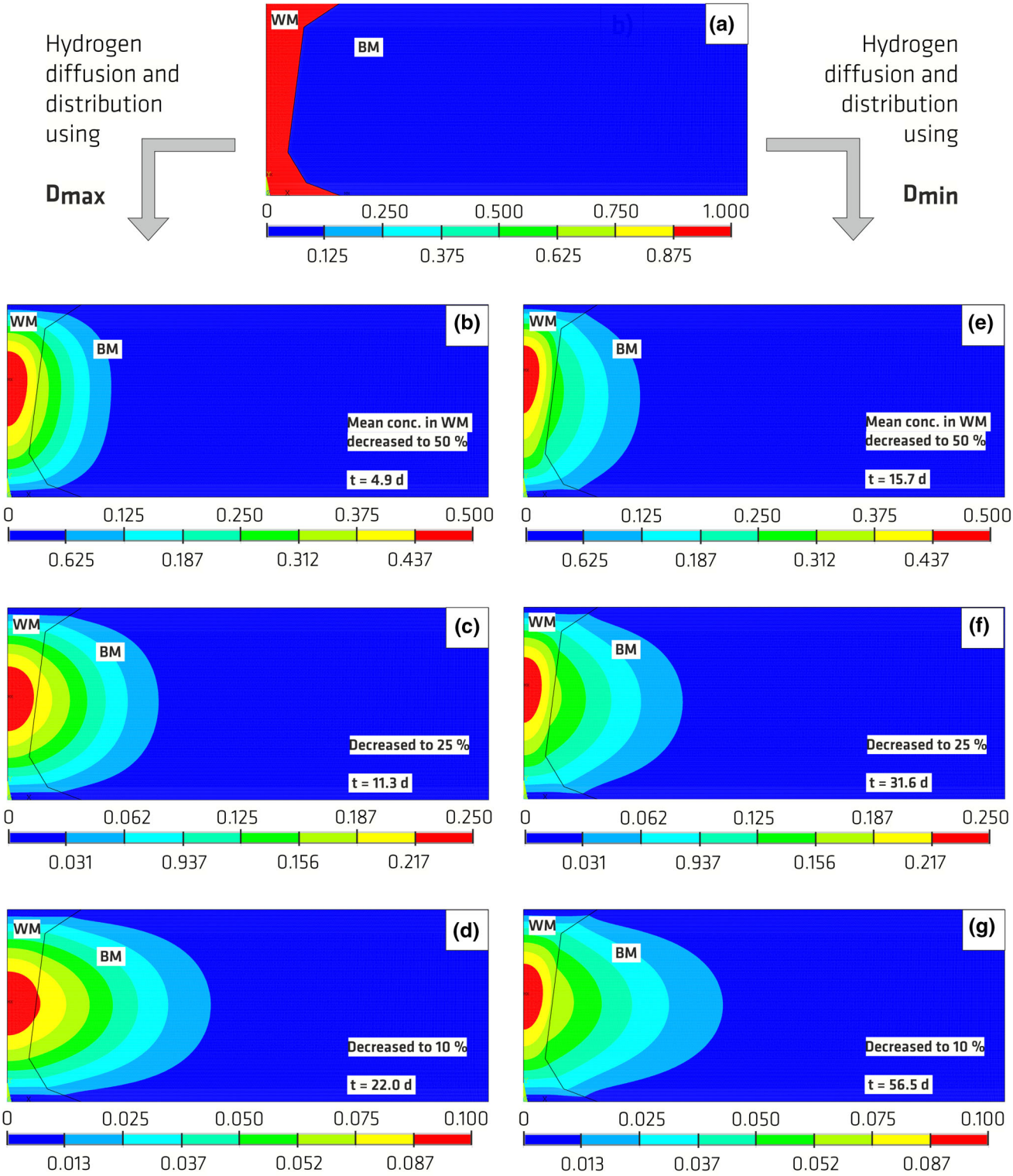

Fig. 12 Simulated diffusion and corresponding hydrogen concentration "*C*": (a) initial concentration 100% (*C* = 1.00) and remaining "*C*" using D_{max} and D_{min}: (b, e) decreased to 50% (*C* = 0.50), (c, f) decreased to 25% (*C* = 0.25) and (d, g) decreased to 10% of initial value (*C* = 0.1) (Color figure online)

$_{WM}$ = 17.40*10^{-5} mm^2/s) 5 days. These decay times are apparently long but have been also numerically validated in (Ref 34). From the viewpoint of any HAC concern, it has to anticipated that our simulation shows the normalized hydrogen concentration, i.e., it can be multiplied with any value as initial concentration. Furthermore, the simulation performed here is a simple approach and represents a worst-case assessment, as the hydrogen concentration in a real welded joint is heterogeneously distributed and already reduced after the weld is

Table 6 Corresponding time to reach 50%, 25% and 10% with D_{min} and D_{max} (of BM and WM)

Concentration after time t Corresponding t using:	Time t for diffusion to reach corresponding hydrogen concentration							
	C = 1.00 (100%)		C = 0.50 (50%)		C = 0.25 (25%)		C = 0.10 (10%)	
	[10^3 s]	[d]	[10^3s]	[d]	[10^3 s]	[d]	[10^3 s]	[d]
D_{min}	600	0.007	1,356	15.7	2,733	31.6	4,878	56.5
D_{max}	600	0.007	424	4.9	979	11.3	1,905	22.0

finished and cooled to ambient temperature due to the thermal cycles during welding (Ref 28).

As mentioned in section 3.2, the current state of the art of SAW typically results in a maximum hydrogen amount of 5 ml/100 g Fe in the weld (H5 classification, see (Ref 16, 20)). In contrast to the suggested fast calculation in section 3.2, case 1, it can be assumed that the highest hydrogen concentration remains in the weld center region (2.5 ml/100g Fe after 16 d or, respectively, 5 d). As mentioned, the mechanical properties of a S690QL steel degrade above ≥ 2.6 ml/100 g (Ref 32). Hence, for the S420G2+M the HAC susceptibility should be significantly decreased at this concentration compared to high-strength steels. The MWT concept should be critically evaluated and confirmed by cold cracking tests of thick-plate welded joints, ensuring realistic mechanical restraints (i.e., residual stresses for cracking).

In addition, in real welds, the introduced hydrogen concentration is neither homogenous nor concentrated at one point. Generally, it assumed that the hydrogen concentration is already significantly reduced compared to the initial value directly after final cooling of the welded joint. The reason is, e.g., the high interpass temperature that is maintained during multi-layer welding of thick-walled components and allows faster hydrogen diffusion (see for example section 3.2, case 2). Our simplified diffusion model resulted in qualitatively similar diffusion times compared to the analytical model but showed that significant differences can also occur. For that reason, numerical modeling is a useful tool for the assessment of HAC (like in accordance with Ref 10–12). But for the simulation of the local time-dependent hydrogen distribution, microstructure-dependent diffusion coefficients like for BM and WM are necessary. More detailed modeling of the different single passes and layers would be beneficial but requires an additional simulation of the welding process with realistic time-temperature curves and especially the cooling time of the single passes (occurring microstructure).

4. Conclusions

In the present study, the hydrogen diffusion in a SAW joint of an offshore grade S420G2+M was investigated for both the base material and weld metal. For this purpose, electrochemical permeation and CGHE experiments had been performed on hydrogen-charged samples. Hydrogen diffusion coefficients were calculated from the obtained experimental data and applied to analytical calculations of the MWT and HRHT dwell time. In addition, a numerical simulation of the time-dependent hydrogen concentration decay was conducted. The following conclusions can be drawn from the results:

- The S420G2+M was investigated the first time in terms of hydrogen diffusion coefficients for BM and multi-layer WM. The coefficients are within the range of 10^{-5} mm^2/s to 10^{-4} mm^2/s at ambient temperature (BM and WM) and 10^{-3} mm^2/s at elevated temperatures (WM).
- In that connection, permeation experiments are a suitable tool to evaluate a MWT via the use of diffusion coefficients. However, the diffusion coefficients changes with sample thickness by up to an order of magnitude. This means that MWT derived from vary accordingly. That means a diffusion coefficient-based MWT does not adequately account for a time-delayed HAC and should be critically discussed.
- The CGHE methodology represents a valuable tool for the determination of high-temperature diffusion coefficients and, e.g., for estimating the dwell times for HRHT. However, for the considered thickness up to 30 mm, very conservative dwell times (longer than one day) result. That means especially for large plate thicknesses, the diffusion path plays a crucial role and can result in long calculated diffusion time.
- A robust analytical calculation of the hydrogen concentration profiles is possible, and only the diffusion coefficient and the initial hydrogen concentration must be known. However, it is disadvantageous as it only represents an approximate solution (assumption: hydrogen concentrated at one point). Further simulations allowed the determination of the local, microstructure and time-dependent hydrogen concentration. Both models clearly showed that reliable diffusion coefficients are necessary for the calculation of the diffusion time.

Acknowledgments

Mr. Lars Gieseler (Erndtebrücker Eisenwerk GmbH & Co.KG, Erndtebrück) is thanked for providing the SAW joints. Mr. Jirka Biermann is thanked for the extensive specimen preparation (EDM) as well as Ms. Marina Marten and Ms. Mareike Kirstein for the metallographic preparation (all with Bundesanstalt für Materialforschung und -prüfung (BAM), Berlin).

Funding

Open Access funding enabled and organized by Projekt DEAL.

References

1. K. Rohing, C. Richts, S. Bofinger, M. Jansen, M. Siefert, S. Pfaffel, M. Durstewitz, Energiewirtschaftliche Bedeutung der Offshore-Windenergie für die Energiewende (in English: Energy-economic impact of the offshore wind energy for the energy transition), Kassel: Fraunhofer-Institut für Windenergie und Energiesystemtechnik (2013)
2. Climate protection program 2030 of the German Federal Government. https://www.bundesregierung.de/breg-de/themen/klimaschutz/klimaschutzprogramm-2030-1673578 (2019)
3. Fraunhofer Institute for Energy Economics and Energy System Technology. Windenergie - Report 2018 (in German, Wind Energy Report 2018), http://windmonitor.iee.fraunhofer.de/opencms/export/sites/windmonitor/img/Windmonitor-2018/WERD_2018_barrierefrei.pdf (2018)
4. DNVGL-OS-C401:2015 Fabrication and testing of offshore structures
5. DIN EN 1090-2: Execution of steel structures and aluminium structures - Part 2: Technical requirements for steel structures, German version EN 1090-2:2018
6. P. Nevasmaa, *Predictive Model for the prevention of weld metal hydrogen cracking in high-strength multipass welds*, University of Oulu, Finland, 2003
7. ISO 17462-1:2004 Destructive tests on welds in metallic materials - cold cracking tests for weldments - Arc welding processes, Part 1: General
8. N. Bailey, F.R. Coe, T.G. Gooch, P.H.M. Hart, N. Jenkins, and R.J. Pargeter, Welding Steels Without Hydrogen Cracking, 2nd ed. Woodhead Publishing (2000)
9. M. Pitrun, D. Nolan, and D. Dunne, Diffusible Hydrogen Content in Rutile Flux-Cored Arc Welds as a Function of the Welding Parameters, *Weld. World.*, 2004, **48**(1/2), p 2–13. https://doi.org/10.1007/BF03266408
10. M. Abe, N. Nakatani, N. Namatame, and T. Terasaki, Influence of Dehydrogenation Heat Treatment on Hydrogen Distribution in Multi-layer Welds of Cr-Mo-V Steel, *Weld. World*, 2012, **56**, p 114–123. https://doi.org/10.1007/BF03321355
11. T. Mente, T. Böllinghaus, and M. Schmitz-Niederau, Heat Treatment Effects on the Reduction of Hydrogen in Multi-layer High-Strength Weld Joints, *Weld. World.*, 2012, **56**(7/8), p 26–36. https://doi.org/10.1007/BF03321362
12. B.T. Alexandrov, Hydrogen Diffusion Coefficient and Modeling of Hydrogen Behavior in Welded Joints of Structural Steels, *Weld. World*, 2003, **47**(9/10), p 21–29. https://doi.org/10.1007/BF0confir66397
13. T. Boellinghaus, H. Hoffmeister, and C. Middel, Scatterbands for Hydrogen Diffusion Coefficients in Steel Having a Ferritic or Martensitic Microstructure and Steels Having an Austenitic Microstructure at Room Temperature, *Weld. World*, 1996, **37**(1), p 16–23
14. R.C. Souza, L.R. Pereira, L.M. Starling, J.N. Pereira, T.A. Simões, J.A.C.P. Gomes, and A.H.S. Bueno, Effect of Microstructure on Hydrogen Diffusion in Weld and API X52 Pipeline Steel and Base Metals Under Cathodic Protection, *Int. J. Corros.*, 2017 https://doi.org/10.1155/2017/4927210
15. Y. Han, H. Jing, and L. Xu, Welding Heat Input Effect on the Hydrogen Permeation in the X80 Steel Welded Joints, *Mater. Chem. Phys.*, 2012, **132**(1), p 216–222. https://doi.org/10.1016/j.matchemphys.2011.11.036
16. A. Swierczynska, and M. Landowski, Plasticity of Bead-on-Plate Welds Made with the Use of Stored Flux-Cored Wires for Offshore Applications, *Materials*, 2020, **13**(17), p 3888. https://doi.org/10.3390/ma13173888
17. S.H. Wang, W.C. Lu, K.F. Ho, and J.K. Wu, Hydrogen Permeation in a Submerged arc Weldment of TMCP Steel, *Mater. Chem. Phys.*, 2003, **77**(2), p 447–454. https://doi.org/10.1016/S0254-0584(02)00100-1
18. E. Ufuah, Characterization of elevated temperature mechanical properties of butt-welded connections Made with HS steel grade S420M, in: Proceedings of the World Congress on Engineering 2012 Vol III, July 4–6, London, UK (2012)
19. DIN EN 10225-1:2019 - Weldable structural steels for fixed offshore structures - Technical delivery conditions - Part 1: Plates, German version EN 10225-1:2019
20. Oerlikon OE-SD3 - SAW Wire, Manufacturer specification (print)
21. Oerlikon OP121TT - SAW flux, Manufacturer specification, https://www.oerlikon-welding.com/de/op-121tt-0
22. ISO 17081:2014 - Method of measurement of hydrogen permeation and determination of hydrogen uptake and transport in metals by an electrochemical technique
23. M. Rhode, *Hydrogen diffusion and effect on degradation in welded microstructures of creep-resistant low-alloyed steels,* BAM-Dissertationsreihe, 148, Bundesanstalt für Materialforschung und -prüfung (BAM), Berlin, Germany (2016)
24. https://physics.nist.gov/cgi-bin/cuu/Value?f: Current definition of Faraday constant in accordance to NIST
25. W. Dresler, and M. Frohberg, Über Ein Vereinfachtes Verfahren zur Bestimmung des Diffusionskoeffizienten von Wasserstoff in Festen Metallen (On a Simplified Method on the Determination of Hydrogen Diffusion Coefficients in Solid Metals), *Int. J Mater. Res.*, 1972, **63**(4), p 204–209
26. F. Iacoviello, J. Galland, and M. Habashi, A Thermal Outgassing Method (TOM) to Measure the Hydrogen Diffusion Coefficients in Austenitic, Austeno-ferritic and Ferritic-pearlitic Steels, *Corros. Sci.*, 1998, **40**(8), p 1281–1293. https://doi.org/10.1016/S0010-938X(97)00145-5
27. M. Mehrer, *Diffusion in Solids - Fundamentals, Methods, Materials, Diffusion-Controlled Processes*, 1st ed. Springer, Germany, 2007
28. T. Boellinghaus, T. Mente, P. Wongpanya, E. Viyanit, and E. Steppan, Numerical modelling of hydrogen assisted cracking in steel welds, *Cracking Phenomena in Welds IV.* T. Boellinghaus, C. Cross Ed., Springer, Cham, 2016
29. M. Rhode, T. Richter, P. Mayr, A. Nitsche, T. Mente, and T. Boellinghaus, Hydrogen Diffusion in Creep-resistant 9% Cr P91 Multi-layer Weld Metal, *Weld. World*, 2020, **64**, p 267–281. https://doi.org/10.1007/s40194-019-00828-8
30. G.M. Pressouryre, A Classification of Hydrogen Traps in Steel, *Metall. Trans. A*, 1979, **10**(10), p 1571–1573. https://doi.org/10.1007/BF02812023
31. G.M. Pressouryre, and I.M. Bernstein, A Quantitative Analysis of Hydrogen Trapping, *Metall. Trans. A*, 1978, **9**, p 1571–1580. https://doi.org/10.1007/BF02661939
32. P. Zimmer, *Zur Bewertung der Kaltrisssicherheit von Schweißverbindungen aus hochfesten Feinkornbaustählen (In English: On the assessment of cold cracking safety of welded joints of high-strength fine-grained steels)*, BAM-Dissertationsreihe, 29, Bundesanstalt für Materialforschung und -prüfung (BAM), Berlin, Germany (2007)
33. E. Wilhelm, T. Mente, and M. Rhode, Waiting Time Before NDT of Welded Offshore Steel Grades Under Consideration of Delayed Hydrogen-Assisted Cracking, *Weld. World*, 2021, **65**, p 947–959. https://doi.org/10.1007/s40194-020-01060-5
34. Y. Yang, G. Liu, and W. Zheng, Study on Hydrogen Diffusion Behavior During Welding of Heavy Plate, *Materials*, 2020, **13**, p 3887. https://doi.org/10.3390/ma13173887